Auxiliary-field quantum Monte Carlo with variational auxiliary-field quantum Monte Carlo trial wave functions

Zixiang Lu
University of Illinois Urbana-Champaign, Champaign, IL, USA

Zhi-Yu Xiao
Institute of Physics, Chinese Academy of Sciences, P.O. Box 603, Beijing 100190, China *

Shiwei Zhang
Center for Computational Quantum Physics, Flatiron Institute, New York, NY 10010, USA †

(Dated: December 4, 2025)

Recent developments [1–3] in auxiliary-field quantum Monte Carlo (AFQMC) show significant potential to further improve its accuracy and efficiency by tethering the branch random walk (BRW) to Markov chain Monte Carlo (MCMC), enabling a scalable implementation of many-body trial wave functions to control the sign problem. One promising choice of such trial wave functions is the variational auxiliary-field quantum Monte Carlo (VAFQMC) [4] wave functions, that optimized in auxiliary-field space to attain efficient sampling and high representational capacity. In this work, we benchmark AFQMC with VAFQMC trial wave functions. Our two-stage framework first optimizes the VAFQMC ansatz via Monte Carlo sampling to capture electronic correlations, then tethers this optimized wave function to AFQMC propagation through stochastic sampling, avoiding costly deterministic expansions. Benchmarking across open-shell atoms (W4-11), main-group molecules (HEAT, W4-MR), heavy lanthanide/actinide atoms (Eu, Tm, Yb; Am, Md, No), and a Cu+ basis-set series shows AFQMC/VAFQMC consistently achieves chemical accuracy (±1 kcal/mol) while reducing biases from traditional trial wave functions (e.g., single/multi-Slater determinant). Our study adapts robustly across reference regimes without system-specific tuning, establishes VAFQMC as a practical, transferable trial wave function for AFQMC, enabling black-box application across chemically diverse systems with consistent accuracy and scalability—bridging accuracy and efficiency in quantum Monte Carlo.

I. INTRODUCTION

Predicting the electronic structure of correlated many-electron systems remains fundamentally challenging[5, 6]. The interplay between kinetic and Coulomb interactions produces rich correlation effects that lie beyond the reach of mean-field or perturbative approaches. Although Density Functional Theory (DFT)[7, 8], Coupled-Cluster methods (CC)[9, 10], Configuration Interaction (CI)[11–13], Density Matrix Renormalization Group (DMRG)[14–16], Dynamical Mean-Field Theory(DMFT)[17–19], Dynamical Matrix Embedding Theory(DMET)[20, 21], and the recently emerged Neural Quantum States (NQS)[22–27] have achieved remarkable progress, no single method offers both systematic accuracy and scalable performance across weakly and strongly correlated regimes. These limitations motivate the development of many-body approaches that can be improved systematically while maintaining practical computational cost.

A prominent example of such many-body approaches is quantum Monte Carlo (QMC)[28, 29], which provides a scalable stochastic framework to describe quantum behaviors. However, the infamous sign problem prevents naive implementation of quantum Monte Carlo from solving many-body problems, especially for systems with strongly correlated electrons, under a scalable cost while maintaining high accuracy. To eliminate the sign problem, one main idea is to enforce a constraint during the Monte Carlo sampling process, resulting auxiliary-field quantum Monte Carlo (AFQMC)[30–35] algorithms, based on a choice of trial wave function, have recently been rapidly developed and widely applied to help the study of quantum many body problems [36–44]. However, the application of constraints usually introduces a small bias corresponding to the choice of trial wave functions. Therefore, further understanding corresponding constraint theories and developing better implementations of AFQMC algorithms to achieve higher accuracy and efficiency are urgent.

Since the choice of trial wave functions and their implementation to resolve such constraints can significantly affect the accuracy and efficiency in AFQMC, related topics have been intensively studied for decades. Traditional studies employ multi-determinant expansions, often based on complete active spaces[36, 45], which recover static correlation but require user-defined active spaces and are sensitive to their choice. Automated constructions, such as natural-orbital expansions[41] and selected configuration interaction (CI) references[37], can systematically approach exactness but at the cost of steep computational scaling and limited black-box us-

* zxiaoMain@outlook.com
† szhang@flatironinstitute.org

ability. Even with screening techniques or DMRG-based references, such approaches do not offer a polynomial-scaling, broadly transferable solution for general systems. Therefore, some work focuses on the design of trial wave function ansatz to maintain a desired balance between low scaling and relatively high accuracy. Symmetry-broken mean-field references (UHF, GHF, unrestricted Kohn–Sham)[39] can capture static correlation at low cost; symmetry projection[42, 43] (e.g., spin or particle-number projection) partially restores good quantum numbers while maintaining high efficiency. Another line of work optimizes the mean-field trial wave function self-consistently using AFQMC one-body density matrices[46], yielding orbital-optimized single- or few-determinant trials without expanding to huge configuration spaces. There are also "single-reference but correlated" inputs—such as CISD[47] or natural-orbital-truncated expansions [41] that avoid manual active-space choices yet remain operationally simple. Despite these developments, a central challenge remains in the compromising of the capability of trial wave function with the efficiency in actual implementation to AFQMC.

One way to intrinsically ease such a struggle is to apply the constraint stochastically. That is, by tethering Metropolis sampled paths to standard AFQMC samples, and dynamically updating these paths to perform the desired constraint along corresponding AFQMC propagation, a large group of trial wave functions (in principle, any wave function that can be evaluated by Monte Carlo) is now possible to be implemented in AFQMC as constraint in a scaled way. Benefiting from such development, the combination between Variational Monte Carlo (VMC)[48] and AFQMC (i.e., take VMC optimized wave function to AFQMC as constraint) can now be seriously considered. A similar idea is commonly used in the study of the first quantized problem, where Diffusion Monte Carlo (DMC) often take the trial wave function optimized by VMC and use fixed-node approximations to perform further projection[49]. In our recent paper[1] and a following paper[2], it has been shown that the variational AFQMC wave function [4] and NNQS can serve as trial wave function of AFQMC, presenting highly accurate results in all tested systems. Since the above prior work mainly focuses on presenting the algorithm, systematic benchmarking of this emergent algorithm is necessary to understand its behavior further.

Though various trial wave functions deserve in-depth investigation, this work focuses on the VAFQMC wave function. A key distinguishing feature of VAFQMC lies in its core design: it treats a short imaginary-time AFQMC propagator as a variational object, where one-body and two-body operator components are optimized jointly with an initial Slater determinant. This formulation eliminates Trotter error (a common limitation of approximate propagators) and typically adopts a single propagation layer in practice, striking a balance between representational expressiveness and computational efficiency. During optimization, VAFQMC samples auxiliary fields to stochastically evaluate and minimize the energy, with a soft sign constraint incorporated to prevent the optimization from collapsing into low-sign regions, yielding an explicitly correlated trial wave function tailored to the system's electronic structure. Notably, VAFQMC operates in an over-complete auxiliary-field space, maintains exceptional computational efficiency (avoiding the exponential scaling of large multi-determinant trials) while retaining high representational capacity to capture both static correlation (e.g., open-shell degeneracy) and dynamical correlation (e.g., short-range electron-electron interactions). This unique synergy of efficiency, correlation-capturing ability, and compatibility with stochastic frameworks makes the VAFQMC wave function a highly appropriate choice for implementation as a constraint in AFQMC calculations.

To systematically investigate the behavior of VAFQMC and its detailed implementation in AFQMC, we first outline the computational framework and validate it on open-shell atoms in the W4-11 dataset [50], comparing the performance of static ROHF trial wave functions and VAFQMC wave functions with different level of Monte Carlo estimation in AFQMC. We then apply the method to main-group molecules in the HEAT and W4-MR datasets and benchmark the resulting AFQMC energies against high-level references. The framework is further tested on heavy lanthanide and actinide atoms (Eu, Tm, Yb; Am, Md, No), where VAFQMC trial wave functions prove substantially more robust than truncated CASSCF trial wave functions. Finally, we analyze the behavior of transition-metal systems through a Cu^+ basis-set study, using channel-power visualizations to characterize the optimized VHS operators and probing the sensitivity of the trial to its capacity and AO-space pruning. Overall, these results establish VAFQMC wave functions as one of the good trial wave functions for AFQMC and provide some practical insights for following more careful designs of VAFQMC trial wave functions.

II. RESULTS

A. Computational Framework

We first outline the computational framework used in this work. Our procedure has two stages (optimization stage and projection stage): we first optimize a VAFQMC ansatz, and then use the optimized ansatz to constrain the following AFQMC projection. The ansatz we employ is a single-slice variational AFQMC (VAFQMC) wavefunction [4, 51, 52], which can be effectively sampled in the auxiliary-field space to describe explicit electronic correlations. Formally, the VAFQMC

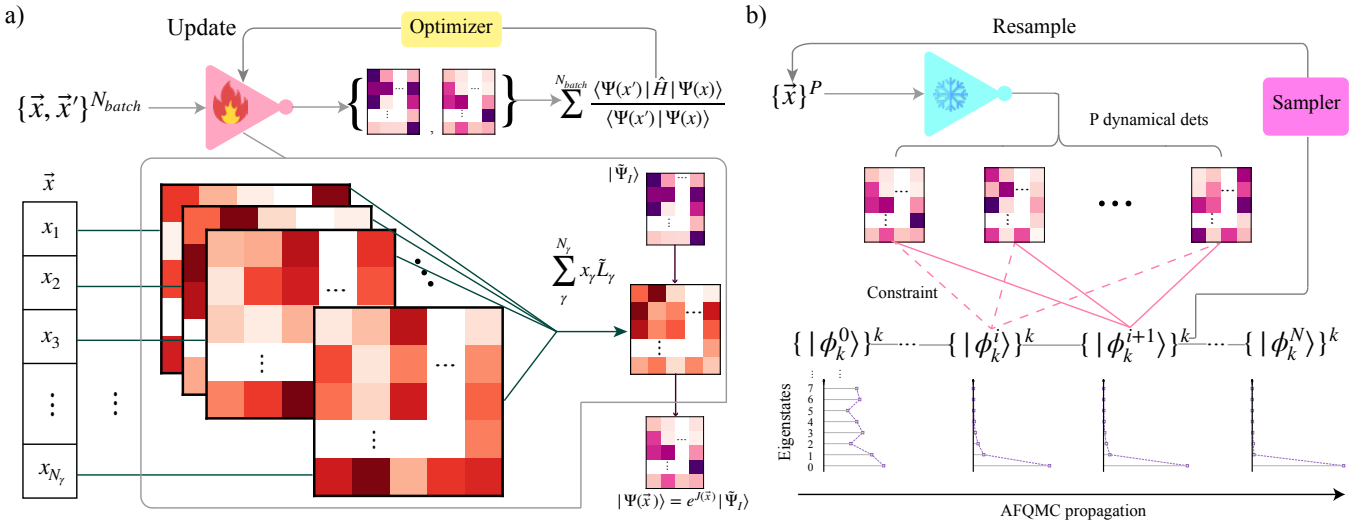

FIG. 1. **Computational framework of this work.**[a] **(a)** Variational optimization of the VAFQMC trial wave function. A batch of sampled auxiliary–field configurations $\{\vec{x}, \vec{x}'\}_{N_{\text{batch}}}$ is used to stochastically evaluate the energy and its gradients, and all variational parameters of the correlated ansatz are updated by the optimizer. Zoom-in: the VAFQMC trial is constructed as a product of exponential one-body propagators, $e^{J}(\vec{x})$, applied successively to an optimizable initial determinant $|\tilde{\Psi}_I\rangle$. The propagator is evaluated through a truncated Taylor expansion $e^{\hat{A}} \approx 1 + \hat{A} + \hat{A}^2/2$, producing the optimized correlated determinant $|\Psi_T(\vec{x})\rangle$. **(b)** Use of the optimized VAFQMC ansatz as a dynamical trial in AFQMC with the phaseless constraint. The optimized ansatz is stochastically resampled to generate P dynamical determinants that constitute the trial manifold enforcing the constraint. During AFQMC propagation, each walker is coupled to a refreshed set of auxiliary fields, yielding updated dynamical determinants that co-evolve with the walker. This leapfrog procedure continuously suppresses excited-state components present in the ensemble-averaged walker state and stabilizes the phaseless constraint, enabling efficient convergence of the projected walkers toward the ground state.

[a] Flame and ice icons in this figure were obtained from Flaticon.com.

ansatz is written as an integral over auxiliary fields,

$$|\Psi_\theta\rangle = \int \prod_\gamma \frac{dx_\gamma}{\sqrt{2\pi}}\, e^{-\frac{1}{2}x_\gamma^2}\, \hat{U}_\theta(x)\, |\tilde{\Psi}_{\mathrm{I}}\rangle, \tag{1}$$

$$\hat{U}_\theta(x) = e^{-\tilde{T}(\theta)}\, e^{\sum_\gamma x_\gamma \tilde{L}_\gamma(\theta)}\, e^{-\tilde{T}_0(\theta)}. \tag{2}$$

Here $|\tilde{\Psi}_{\mathrm{I}}\rangle$ can be a parameterized linear combination of Slater determinants (for simplification, this work only use a Slater determinant), and all operator blocks $\tilde{T}_0(\theta), \tilde{T}(\theta), \tilde{L}_\gamma(\theta)$ carry variational parameters. Although the formal ansatz in Eqs. (1)–(2) contains both one- and two-body operator blocks, in Fig. 1(a) we depict only the auxiliary-field channels $\{x_\gamma, \tilde{L}_\gamma\}$. Integration of all these channels constitutes the dominant correlation-carrying component of the ansatz, analogizing the Jastrow correlation factor in a Slater–Jastrow wavefunction. The one-body terms $\tilde{T}_0$ and $\tilde{T}$ are absorbed into the surrounding linear transformations of the determinant in practice and are omitted from the schematic for clarity.

In the optimization stage, we optimize $|\Psi_\theta\rangle$ by Monte Carlo sampling pairs of field configurations (x, x') and minimizing the stochastic energy with a soft sign constraint. For more details of VAFQMC, refer to [4]. This stage yields an explicitly correlated, walker-compatible trial wave function $\langle\Psi_T|$ that lives in the auxiliary-field space. In the second projection stage (Fig. 1(b)), this trial wave function is tethered to each AFQMC walker (i.e., Slater determinant that sampled propagated by standard AFQMC procedure). The actual AFQMC and constraint procedures are determined by the overlap ratios between the trial wave function and the corresponding AFQMC walker. Thus, by implementing Monte Carlo sampling (Metropolis algorithm here) to estimate such overlap ratios dynamically along the propagation of AFQMC, we provide a rigorous application of the constraint described by the desired VAFQMC trial wave function, avoiding a costly deterministic expansion.

To further enhance scalability, we extended the original VAFQMC implementation to a distributed multi-GPU framework. Independent Monte Carlo samples are assigned to different GPUs and communicate only through lightweight reductions of observables, preserving stochastic independence while achieving near-linear strong scaling across devices. Leveraging JAX's functional programming model and automatic parallelization primitives [53], this distributed design can be implemented with minimal overhead, enabling us to treat substantially larger molecular and transition-metal systems than previously feasible.

Once the variational parameters are converged, we freeze them and use the resulting state as the trial wave function for the following projection stage, denoted

the optimized ansatz as $|\Psi_T\rangle$. In the projection stage (Fig. 1(b)), the two-step leap-frog move is applied to update the samples of trial wave functions and AFQMC walkers, and provides a fair evaluation for the overlap ratios. For a walker state $|\phi_k^i\rangle$ at imaginary-time step i, we form

$$\frac{\langle\Psi_T|\phi_k^{i+1}\rangle}{\langle\Psi_T|\phi_k^i\rangle},$$

and based on this ratio to implement the importance sampling and the phaseless gauge as described standard phaseless AFQMC [32]. Because $|\Psi_T\rangle$ was sampled and optimized in the Slater determinant manifold, these evaluations of overlaps can be performed with the same determinant machinery as in the variational stage. For a detailed implementation, refer to our previous paper[1].

The variational optimization in VAFQMC requires repeated evaluations of the energy functional and its gradients, each involving Slater determinant updates and contractions over the Cholesky factors and therefore scaling as $O(N^3)$ with the number of basis functions N. The total optimization cost is $O(N^3 N_{\text{conv}})$, where N_{conv} denotes the number of optimization iterations. Consistent with experience in variational Monte Carlo, N_{conv} exhibits only weak dependence on system size and is well approximated by $N_{\text{conv}} \propto N^\beta$ with $\beta \lesssim 1$ for chemically relevant systems. Following optimization can be done by taking the advantages that each Metropolis proposal only modifies a small subset of auxiliary fields and requires no recomputation of determinant ratios, Green's functions, or Cholesky contractions, resulting in a subcubic cost $O(N^\alpha)$ with $1 \le \alpha \le 2$. Even with P sampled paths and M updates per AFQMC time step, this overhead remains negligible relative to the $O(N^3)$ AFQMC propagation. Thus, AFQMC with dynamical trials is effectively equivalent to AFQMC employing a P sampled paths while preserving the cubic dependence on N. Collecting all contributions, the overall computational complexity of the combined VAFQMC–AFQMC framework may be summarized as

$$T_{\text{total}} = O(N^{3+\beta}) + O(PN^{3+\gamma}),$$

where $N_\tau \propto N^\gamma$ with $\gamma \lesssim 1$ denotes the number of AFQMC projection steps. Hence, the introduction of VAFQMC trial wave funtions preserves the favorable cubic scaling of AFQMC while introducing only modest prefactors from trial optimization and sampling.

This design of above allows the projector (i.e., AFQMC) to benefit from a trial wave function that is already adapted to the system's correlation, while the AFQMC propagation further reduces the residual bias from the optimization stage. In theory, such a framework allows any wave function that can be sampled by Monte Carlo to be integrated with AFQMC. In practice, systematic benchmarking across diverse systems is essential to understand their effects on the detailed choice of parameters and VAFQMC ansatz, which is directly tied to the computational cost (mainly the choice of sampled paths P), optimization difficulties and will help following extensive applications of related methods. In the following, we present a systematic benchmark study of the new algorithm. We will use **VAFQMC** to denote the variationally optimized ansatz, and **AFQMC/VAFQMC** to denote the following AFQMC calculations with VAFQMC trial wave functions. More detailed parameters and setup are summarized in APPENDIX.

B. Application to Small Atoms

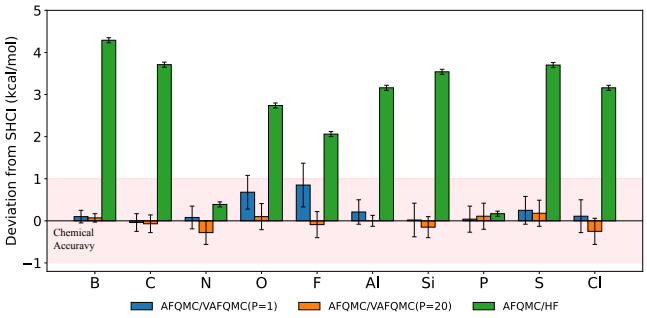

FIG. 2. **Absolute deviations (in kcal/mol) from SHCI reference energies for different trial wave functions.** The green bars represent AFQMC calculations using ROHF single-determinant trial wave functions, the blue and orange bars correspond to AFQMC with VAFQMC trial wave functions (AFQMC/VAFQMC) but different numbers of sampled paths P. All AFQMC/VAFQMC results fall within chemical accuracy. The SHCI reference and ROHF-based AFQMC data are taken from Ref. [54]. All calculations were performed in the aug-cc-pVTZ basis set.

To demonstrate the basic framework and effectiveness of AFQMC/VAFQMC, we first examine the total energies of small atoms from the W4-11 dataset [50]. Previous studies [54] reported that AFQMC with ROHF trial wave functions exhibit sizable systematic bias for open-shell atoms, particularly for systems with non-zero angular momentum, and achieving chemical accuracy in such cases typically requires hundreds of determinants.

In Fig. 2, we report high accuracy of AFQMC with VAFQMC trial wave functions in W4-11 dataset, using a small number of sampled paths to characterize VAFQMC trial wave functions. Even a sample (i.e., analog to using a dynamically updated single-determinant trial wave function) is enough to attain chemical accuracy. Throughout all tested cases in the W4-11 dataset, computed total energies agree with the reference SHCI values within chemical accuracy (1 kcal/mol), effectively eliminating the bias associated with static single-determinant trial wave function.

The failure of ROHF trial wave functions comes from its static implementation (i.e., fixed at one symmetry-breaking state in the whole AFQMC propagation). In-

stead of involving hundreds of determinants to recover the open shell degeneracy, a more efficient choice, as we did here, is to allow symmetry-breaking state to be updated dynamically and recover the degeneracy stocastically. For systems that mainly suffer from such an open-shell problem, as demonstrated in Fig. 2, AFQMC/VAFQMC can effectively solve it by using a small number of sampled paths, even one path (i.e., $P = 1$), to recover open-shell degeneracy and systemically improve the accuracy with minimal cost.

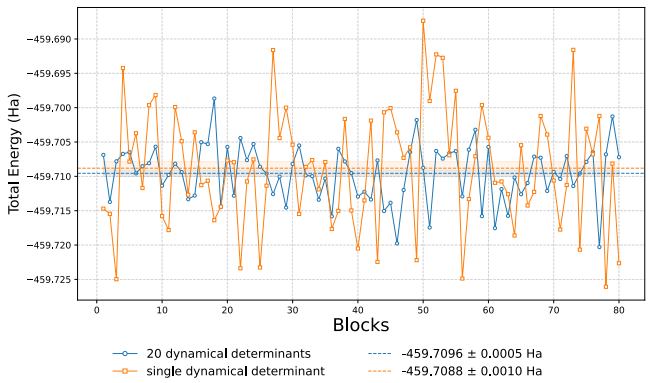

FIG. 3. AFQMC block-averaged total energies for the Cl atom using the same VAFQMC trial wave functions but different sampled paths: $P = 20$ (orange) versus $P = 1$ (blue). Each marker is one estimation block after equilibration. Dashed lines denote the sample means; the legend reports mean ± one–standard-error. With the same number of blocks (80), the single-determinant trial shows about twice the statistical uncertainty (~ 1 mHa) and visibly larger block-to-block fluctuations than the 20-determinant trial (~ 0.5 mHa).

Because the implementation of the VAFQMC trial wave function to AFQMC is resolved through Monte Carlo sampling, extra stochastic/systemcatic error is introduced, especially when only a sampled path (i.e., $P = 1$) is used. As shown in Fig. 3, the AFQMC energy for Cl obtained with $P = 1$ exhibits markedly larger block-to-block fluctuations than with $P = 20$, so more blocks are required to reach the same precision. Running for 80 blocks in both cases, the $P = 1$ run yields an error bar of ≈1 .mHa, roughly twice that of the $P = 20$ run (≈0.5 .mHa). Extending the $P = 1$ simulation to ∼240 blocks reduces its error bar to a comparable level. Population-control effects also become more pronounced under stronger phaseless fluctuations, intermittently removing additional walkers and adding variance. These effects are substantially eased by increasing the number of sampled paths P; in practice, using about $P = 20$ is sufficient, and we adopt this setting in subsequent larger or more strongly correlated systems.

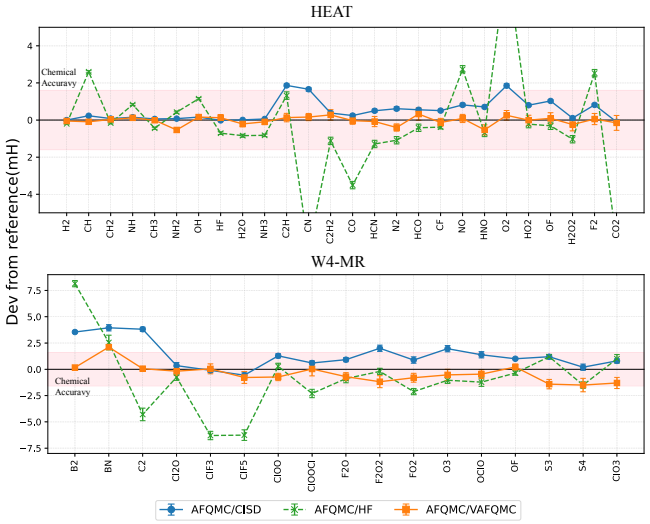

FIG. 4. Deviation of the AFQMC total energies obtained using VAFQMC, Hartree–Fock, and CISD trial wave functions across the HEAT and W4-17-MR benchmark molecules in cc-pVDZ basis. For both datasets, the AFQMC/CISD results are taken from Ref. [47]. For the HEAT dataset, the CCSDTQP reference values are from Ref. [55], and the AFQMC/HF data are from Ref. [56]. For the W4-17-MR dataset, both the reference values and the AFQMC/HF data are taken from Ref. [47].

.

Dataset	AFQMC/HF	AFQMC/CISD	AFQMC/VAFQMC
HEAT	2.84	0.75	0.22
W4-MR	3.33	1.87	0.93

TABLE I. RMSD (mHa) of AFQMC energies using Hartree–Fock, CISD, and VAFQMC trials across the HEAT and W4-MR datasets.

C. Application to main group molecules

To investigate the performance of AFQMC/VAFQMC in more sophisticated systems, we evaluate our approach using two established benchmarks, HEAT[57] and the strongly multireference subset W4 (W4-MR)[58], both of which present stringent tests for many-body electronic-structure methods. The HEAT set consists mainly of first-row species with relatively mild multi-reference character, whereas W4-MR was explicitly designed to contain systems dominated by strong static correlation that require high-level multi-reference representation. Together, these datasets provide a consistent and widely adopted reference for assessing correlated wave function methods. For comparison, we include AFQMC calculations using Hartree–Fock (AFQMC/HF) and CISD-based (AFQMC/CISD) trial wave functions. The AFQMC/HF provides the simplest single-reference baseline for AFQMC algorithms, while the AFQMC/CISD in recent AFQMC studies [47] is referred to as the latest state-of-the-art AFQMC benchmarking results. These

baselines establish a clear context for quantifying the additional accuracy afforded by the variationally optimized VAFQMC ansatz. All calculations employ a uniform set of parameters across all species for both VAFQMC and AFQMC, ensuring that the performance of the method is assessed under a consistent computational protocol rather than system-dependent tuning. Detailed parameters are presented in APPENDIX. Furthermore, to remain consistent with Ref. [47], we freeze the He core for second-row atoms and the Ne core for third-row atoms in all calculations.

Across the HEAT dataset, AFQMC/VAFQMC show uniformly small and tightly bounded deviations relative to the reference values. No chemical subgroup displays noticeably larger errors, indicating that the method maintains a stable constraint throughout the set and adapts reliably even in comparatively simple electronic environments. The W4-17-MR dataset presents a more challenging test, with an overall RMSD of 0.93 mHa , yet most of the results still fall within chemical accuracy. A mild trend appears for the larger and more strongly correlated molecules, such as S_3, S_4, and ClO_3, where the deviations increase slightly. This behavior is consistent with the expectation that, under fixed optimization parameters, the variationally optimized trial may not retain the same level of quality as in smaller systems.

Taken together, these results highlight an essential feature of the approach: the implementation of VAFQMC trial wave functions significantly reduces constraint variability across chemically diverse systems. The method performs consistently from single-reference to strongly multireference regimes while maintaining a low computational overhead. The HEAT and W4-MR benchmarks therefore illustrate that the central advantage of AFQMC/VAFQMC lies not in targeting any specific class of molecules, but in providing a generally robust trial formulation that maintains accuracy across heterogeneous chemical environments.

D. Heavy Atoms

Heavy atoms—the lanthanides and actinides—are known to be challenging for many-body methods. Their large valence manifolds contain nearly degenerate d and f orbitals, so that valence electrons can delocalize across several competing shells, generating strong static correlation on top of substantial dynamical correlation. High-level benchmarks for isolated f-block atoms have therefore relied on relativistic coupled-cluster and composite schemes together with correlation-consistent X2C basis sets, which deliver chemically accurate ionization potentials and energetics across the La–Lu and Ac–Lr series.[59–61] In such a regime, a simple single-reference description is unreliable, while straightforward multireference expansions become extremely large and sensitive to the precise choice of active space.

As a compact yet representative subset, we consider

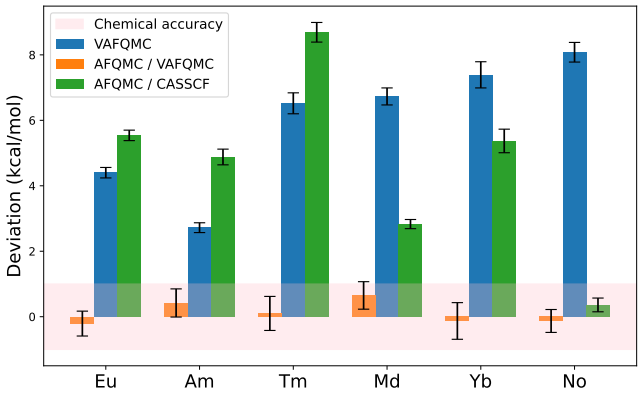

FIG. 5. Deviation (kcal/mol) of VAFQMC, AFQMC/VAFQMC, and AFQMC/CASSCF from high–order coupled–cluster (HOCC) reference energies for six lanthanide and actinide atoms. The shaded band marks the chemical-accuracy window (±1 kcal/mol).

six atoms spanning both series and the three canonical f-shell regimes: Eu and Am (half-filled), Tm and Md (nearly filled), and Yb and No (closed shell). This set includes both open- and nominally closed-shell cases and captures the main sources of difficulty: near-degeneracy among $f/d/s$ shells, core–valence correlation, and strong sensitivity of the nodal/phase structure of any trial state. We keep the one-particle ingredients fixed at the scalar-relativistic X2C level with the cc-pVDZ-X2C basis,[59, 60] and construct HOCC reference energies using a hierarchy of coupled-cluster truncations in the spirit of the heavy-element benchmarks above, but applied uniformly to all six atoms. Localized $4f/5f$ shells embedded in dense valence manifolds make the absolute total energies highly sensitive to the balance between non-dynamical and dynamical correlation, so this provides a stringent test for any trial-dependent projector method.

Figure 5 summarizes our results under the X2C/cc-pVDZ-X2C setup. For the actinides (Am, Md, No) we correlate the $\{6s, 6p, 7s, 5f\}$ shells and freeze all deeper orbitals; for the lanthanides (Eu, Tm, Yb) we analogously correlate $\{5s, 5p, 6s, 4f\}$ and freeze all deeper shells. At the purely variational level, the optimized VAFQMC ansatz still deviates from the HOCC reference by several kcal/mol for some of these atoms, reflecting the extreme sensitivity of f-shell energetics. However, when we stochastically sample $p = 20$ determinants from the VAFQMC state and use them as the AFQMC trial (AFQMC/VAFQMC), the resulting AFQMC energies are consistently within chemical accuracy for all six atoms. By contrast, AFQMC with a truncated CASSCF trial (AFQMC/CASSCF), built from an active space that nominally covers the f-shell manifold and truncated to 10,000 determinants, is systematically less accurate and often lies outside the chemical-accuracy band; pushing the CASSCF truncation to even larger determinant counts does not lead to a clear systematic improvement

within practical cost. These results indicate that a dynamically sampled VAFQMC trial can effectively replace extremely large static multireference expansions and provides a practical, high-accuracy option for heavy-atom benchmarks and f-element chemistry.

E. Cu^+ basis behavior and trial sensitivity

Transition-metal systems remain prototypical testbeds for strong correlation and continue to challenge standard quantum-chemistry approximations. Prior AFQMC benchmarks have shown that truncated CASSCF multideterminant trials can still leave non-negligible bias for these molecules [62, 63]. Our recent work demonstrated that AFQMC with a stochastically sampled VAFQMC trial wave functions systematically attains chemical accuracy for a panel of transition-metal diatomics in a modest basis [1]. Here we examine how this approach behaves in larger bases and how sensitive it is to the quality of the optimized VAFQMC ansatz.

We take Cu^+ as a representative case. Using the same VAFQMC and AFQMC hyperparameters across all calculations, we first optimize the VAFQMC ansatz to convergence and then employ it as the trial wave function in AFQMC. We compare directly to near-exact SHCI energies from Ref. [62] under identical settings (equilibrium geometry, pseudopotential, and basis sets). Figure 6(a) reports deviations from SHCI for four bases (vdz, vtz, vqz, v5z). It is surprising that for such a hard problem, VAFQMC (green) can track the reference within a few kcal/mol. When used as trial wave functions, AFQMC/VAFQMC (orange) yields residual errors consistently within the chemical-accuracy band for all bases. By contrast, AFQMC/CASSCF (blue) retains a systematic underestimation of ∼3–5 kcal/mol across bases.

To investigate the relatively high accuracy of the VAFQMC wave function, we proceed in two steps to make the effect of variational optimization directly visible. First, we transform the optimized operators from the canonical molecular–orbital (MO) basis, where both VAFQMC and AFQMC are formulated—back to the atomic–orbital (AO) basis. This eliminates system–dependent MO rotations and allows structural patterns in the auxiliary fields to be compared on a common, chemically meaningful basis. Notably, all VAFQMC calculations in this work used the Hamiltonian of our target system as the initial parameters (as presented in Fig.6 b, that denoted by "Initial"), and we believe this initial condition can lead to some specific observation below. As presented in APPENDIX, each individual VHS channel appears remarkably sparse and localized in the AO basis, indicating that every L_γ captures only a specific fragment of the total correlation structure rather than acting as a fully delocalized operator. Next, we aggregate the full set of auxiliary one–body operators $\{L_\gamma\}_{\gamma=1}^{\Gamma}$ (the "VHS" channels produced by the modified–Cholesky factorization) into a single heatmap as shown in Fig.6 b. Although the Cholesky procedure initializes different channels with different numerical scales, within the VAFQMC framework all channels are treated as trainable parameters on an equal footing. We therefore combine them uniformly by forming a channel–power map,

$$P_{ij} = \Big(\sum_{\gamma=1}^{\Gamma} [L_{\gamma,ij}]^2\Big)^{1/2},$$

which measures how strongly each pair of orbitals (i, j) is coupled across all auxiliary channels. For each setting (initial/optimized), we apply a single global Frobenius normalization to the whole stack $\{L_\gamma\}$ so that the heatmaps emphasize structure rather than overall scale. All magnitude panels share a common color scale, and we omit numeric annotations since the visual goal is pattern recognition.

To summarize the change compactly, we compute a stabilized relative change,

$$\Delta_{ij} = \frac{P_{\mathrm{opt},ij} - P_{\mathrm{init},ij}}{P_{\mathrm{init},ij} + \tau},$$

with a small stabilizer $\tau = 10^{-6} \times \mathrm{median}\big(P_{\mathrm{init}}^{(B)}\big)$ to avoid division–by–near–zero artifacts; entries where both P_{init} and P_{opt} fall below the joint 10th percentile are masked. The difference map (right column) highlights that, in the AO representation, the adjustments are highly localized: the vast majority of matrix elements exhibit $|\Delta_{ij}| \lesssim 0.05$, while sizeable updates $|\Delta_{ij}| \gtrsim 0.1$ appear only in a few compact clusters associated with valence p–, d–, and f–shell subblocks. The s block and core–valence couplings remain essentially unchanged, indicating that the optimization mainly refines the correlation structure within and between valence manifolds rather than reorganizing the global block pattern.

To probe how the quality/size of the VAFQMC trial wave function impacts following AFQMC accuracy, we reduce the number of trainable VHS operators in the ansatz to $n_{\mathrm{vhs}} \in \{10, 30, 50, 70, 90, 100\}$. For each n_{vhs} we optimize the VAFQMC energy to convergence on the `vdz` basis, and then use the optimized ansatz as the AFQMC trial wave function. Figure 6(c) reports deviations from SHCI (Ha). As expected, the variational error decreases monotonically with n_{vhs} since the expressiveness of the corresponding VAFQMC ansatz (i.e., n_{vhs}) decreases. AFQMC calculations follow the same trend but remain within chemical accuracy only when the expressiveness of the ansatz is not overly reduced: as n_{vhs} decreases the AFQMC/VAFQMC deviation grows and, in our `vdz` test, it leaves the ±1 kcal/mol band ($\pm 1.593 \times 10^{-3}$ Ha) once $n_{\mathrm{vhs}} < 90$. The results caution against aggressive pruning of n_{vhs}.

Motivated by the AO sparsity observed in Fig. 6(b), we performed a second test in which we start from the well–optimized VAFQMC wave function, rotate the VHS to the AO basis, and then within each $L_\gamma^{(\mathrm{AO})}$ zero out a

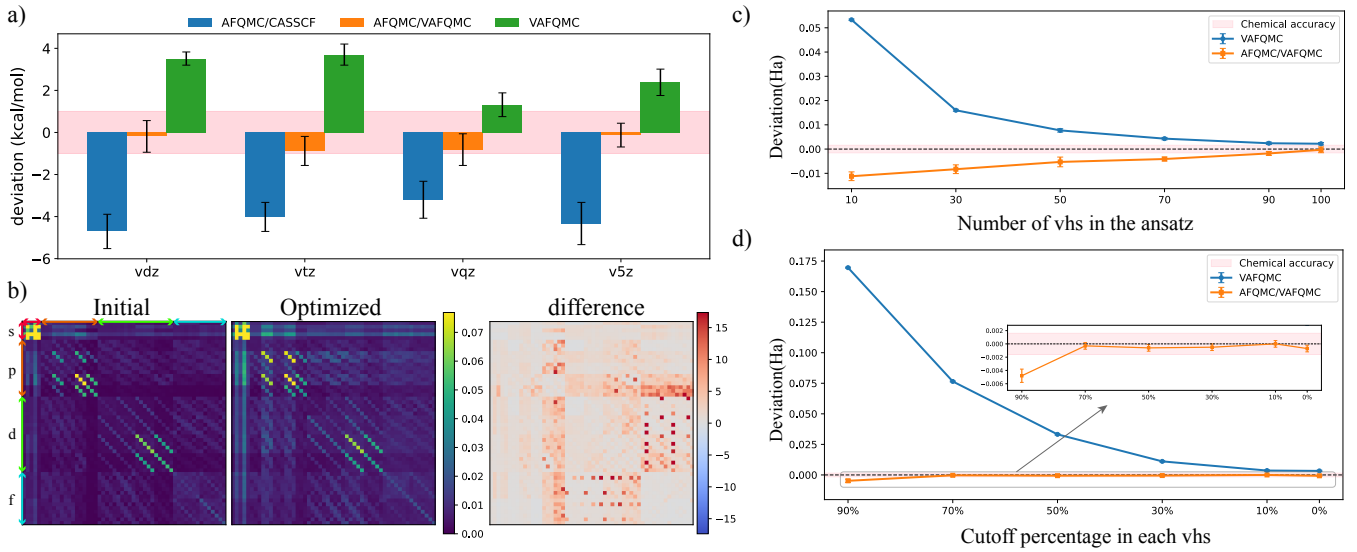

FIG. 6. **Cu^+ basis-set study. (a)** Deviations from SHCI (kcal/mol) for four basis sets. The shaded band marks the chemical-accuracy window (±1 kcal/mol). Blue: AFQMC with truncated CASSCF trials (AFQMC/CASSCF). Orange: AFQMC with stochastically sampled VAFQMC trials (AFQMC/VAFQMC). Green: variational VAFQMC energies (trial energies). SHCI reference energies, basis-set and pseudopotential settings, and the AFQMC/CASSCF data are taken from Ref. [62]. **(b)**Visualization of VAFQMC trial operators in vdz basis. Each panel shows the channel–power map $P_{ij} = \left(\sum_\gamma L_{\gamma,ij}^2\right)^{1/2}$ aggregated from the VHS operators $\{L_\gamma\}$. AO panels are labeled by $s/p/d/f$ blocks. Left and middle columns display the initial (chunked Cholesky) and optimized parameters, respectively, after a single global Frobenius normalization of each stack; magnitude panels share a common color scale. The right column shows the difference of the initial and optimized vhs. **(c)** Deviations from SHCI (Ha) for the variational energy (VAFQMC, blue) and for AFQMC using the optimized VAFQMC trial (AFQMC/VAFQMC, orange) as a function of the number of trainable VHS operators $n_{\rm vhs} \in \{10, 30, 50, 70, 90, 100\}$ on the `vdz` basis. **(d)** Deviations from SHCI (Ha) versus AO–basis elementwise cutoff percentage $p \in \{90, 70, 50, 30, 10, 0\}\%$ applied to each VHS operator: starting from the optimized trial ($n_{\rm vhs} = 100$), the operators are rotated to the AO basis, within each $L_\gamma^{\rm AO}$ the smallest $|\cdot|$ entries at rate p are set to zero, and the operators are rotated back to the canonical MO basis; no further optimization is performed. The inset provides a zoom of the AFQMC/VAFQMC curve near zero.

fixed percentage $p \in \{10, 30, 50, 70, 90\}\%$ of the smallest $|\cdot|$ entries (keeping the largest ones). We then rotate back to the canonical MO basis and, without any further optimization, evaluate the variational energy of this pruned VAFQMC wave function and, use it as the AFQMC trial wave function. As shown in Fig. 6d), the VAFQMC(trial) energy deteriorates rapidly with p because many small–magnitude AO entries are removed; however, the corresponding AFQMC energy is remarkably robust and stays within the chemical–accuracy band up to about $p = 90\%$. This behavior is consistent with the view that pruning in AO mainly discards weak, long–range couplings while leaving the dominant local structure largely intact, hence the sign/phase information most relevant for the constraint. The above studies suggest a large room for further improvement in the optimization strategies and design of scalable ansatz that target trial wave functions which are compact yet retain the essential sign/phase structure, thereby reducing computational cost while maintaining high AFQMC accuracy.

III. SUMMARY AND DISCUSSION

The present work demonstrates that VAFQMC can provide an efficient and transferable strategy for constructing trial wave functions for AFQMC. By optimizing the ansatz directly in auxiliary–field space and sampling a small determinant manifold dynamically, the resulting AFQMC/VAFQMC scheme achieves advanced performance across chemically diverse systems—including open-shell atoms, main-group molecules, heavy lanthanides and actinides, and transition-metal, without system-specific active-space choices or tailored hyperparameters.

The behavior of the auxiliary one–body operators $\{L_\gamma\}_{\gamma=1}^{\Gamma}$ in the AO basis further clarifies the mechanism: optimization chiefly reorganizes short-range couplings while preserving the global operator structure, yielding a trial that stabilizes the phaseless constraint even when the variational energy alone is not perfect. Together with our benchmarking results that only take a small number of sampled paths (i.e., $P = 20$), it suggest that the primary requirement for an effective AFQMC trial wave function is not a highly accurate description of the ground state but a faithful representation of the

sign structure relevant to the constraint, which the auxiliary–field formulation and corresponding simple Monte Carlo sampling can naturally capture.

These findings motivate a broader perspective on combining variational optimization with projector methods. The VAFQMC stage provides a correlated, system-adaptive reference of modest dimension, while the AFQMC projection efficiently removes remaining variational bias. This separation of roles preserves the favorable polynomial scaling of AFQMC and enables straightforward deployment on distributed multi-GPU architectures. The observed AO sparsity and robustness to operator pruning suggest opportunities for more structured or sparsity-promoting parameterizations, including symmetry-equivariant forms and neural-network augmentations of the VHS manifold.

Overall, the results show that VAFQMC together with AFQMC constitute a reliable and scalable approach, yielding consistently improved accuracy across both weakly and strongly correlated systems even when employed in a straightforward, black-box manner. Moreover, as a variationally optimized wave function, the VAFQMC form naturally accommodates alternative objective functions, allowing the optimization to target specific electronic states[64, 65] when desired and providing a versatile protocol for future applications. We believe the introduction of the VAFQMC/AFQMC framework and our test can help future work to further understand and use the hidden mechanism of constraint in AFQMC and thus the study of many-body problems.

IV. METHODS

In this section, we briefly introduce the methods we use to perform the AFQMC with VAFQMC trial wave function. For the details regarding the implementation, please refer to [1, 4].

Variational auxiliary-field ansatz

We employ a variational auxiliary-field quantum Monte Carlo (VAFQMC) ansatz to construct a compact yet expressive correlated wave function. The central idea is to treat a short imaginary-time AFQMC propagator as a variational object whose one-body and two-body components are optimized jointly with the initial Slater determinant. The resulting state takes the continuous form

$$|\psi_\theta\rangle = \exp\!\left[-\int_0^\tau \tilde{H}(s)\,\mathrm{d}s\right]\left|\tilde{\psi}_I\right\rangle, \tag{3}$$

where θ denotes all variational parameters. After discretization and a Hubbard–Stratonovich decoupling, the ansatz becomes an integral over auxiliary fields,

$$|\psi_\theta\rangle = \int\left(\prod_{\gamma,l}\frac{\mathrm{d}x_{\gamma l}}{\sqrt{2\pi}}e^{-x_{\gamma l}^2/2}\right)\left(\prod_{l=1}^{N_l} e^{-t_l\tilde{T}_l}\, e^{\sqrt{-s_l}\sum_{\gamma=1}^{N_\gamma} x_{\gamma l}\tilde{L}_\gamma}\right) \times e^{-t_0\tilde{T}_0}\left|\tilde{\psi}_I\right\rangle \equiv \int \mathrm{d}\mathbf{x}\,\tilde{U}(\mathbf{x})\left|\tilde{\psi}_I\right\rangle, \tag{4}$$

with $\mathbf{x} = \{x_{\gamma l}\}$ and $\{t_l, s_l\}$ denoting optimizable step sizes. Because the full propagator is treated variationally, the ansatz is free of Trotter error and admits relatively large time steps; in practice we adopt a single propagation layer ($l = 1$), which yields a favorable balance between expressiveness and computational efficiency.

The variational parameters are obtained by minimizing the projected energy

$$E_\theta = \frac{\displaystyle\int \mathrm{d}\mathbf{x}\,\mathrm{d}\mathbf{x}'\,\langle\tilde{\psi}_I|\tilde{U}^\dagger(\mathbf{x}')\hat{H}\tilde{U}(\mathbf{x})|\tilde{\psi}_I\rangle}{\displaystyle\int \mathrm{d}\mathbf{x}\,\mathrm{d}\mathbf{x}'\,\langle\tilde{\psi}_I|\tilde{U}^\dagger(\mathbf{x}')\tilde{U}(\mathbf{x})|\tilde{\psi}_I\rangle}. \tag{5}$$

For Monte Carlo evaluation, each overlap is decomposed into its magnitude $\mathcal{D}$, phase $\mathcal{S}$, and local energy $\mathcal{E}$,

$$\mathcal{D}(\mathbf{x},\mathbf{x}') = \left|\langle\tilde{\psi}_I|\tilde{U}^\dagger(\mathbf{x}')\tilde{U}(\mathbf{x})|\tilde{\psi}_I\rangle\right|, \tag{6}$$

$$\mathcal{S}(\mathbf{x},\mathbf{x}') = \frac{\langle\tilde{\psi}_I|\tilde{U}^\dagger(\mathbf{x}')\tilde{U}(\mathbf{x})|\tilde{\psi}_I\rangle}{\mathcal{D}(\mathbf{x},\mathbf{x}')}, \tag{7}$$

$$\mathcal{E}(\mathbf{x},\mathbf{x}') = \frac{\langle\tilde{\psi}_I|\tilde{U}^\dagger(\mathbf{x}')\hat{H}\tilde{U}(\mathbf{x})|\tilde{\psi}_I\rangle}{\langle\tilde{\psi}_I|\tilde{U}^\dagger(\mathbf{x}')\tilde{U}(\mathbf{x})|\tilde{\psi}_I\rangle}. \tag{8}$$

The energy then becomes

$$E_\theta = \frac{\langle\mathcal{E}\mathcal{S}\rangle_\mathcal{D}}{\langle\mathcal{S}\rangle_\mathcal{D}}. \tag{9}$$

To stabilize the optimization against sign fluctuations, we penalize reductions of the average sign

$$S_\theta = \mathrm{Re}\big[\langle\mathcal{S}\rangle_\mathcal{D}\big], \tag{10}$$

and minimize the augmented objective

$$\min_\theta\big[E_\theta + \lambda\max(B - S_\theta,\,0)^2\big], \tag{11}$$

with fixed $\lambda = 1$ and $B = 0.7$. This soft constraint preserves variational integrity while preventing the optimization from collapsing into low-sign regions of configuration space.

AFQMC with VAFQMC as trial wave function

The optimized VAFQMC state provides an effective trial wave function for phaseless AFQMC. Although expressed compactly as a single variational propagator, the

ansatz expands into an auxiliary-field–dependent linear combination of Slater determinants,

$$|\psi_\theta\rangle = \int \mathrm{d}\mathbf{x}\, \tilde{U}(\mathbf{x}) \left|\tilde{\psi}_I\right\rangle, \tag{12}$$

so that every evaluation of overlaps or local energies requires sampling a new set of fields $\mathbf{x}$. In practice, AFQMC therefore interacts not with a fixed trial determinant, but with a dynamical single- or multi-determinant representation whose composition changes along AFQMC propagation. This provides access to many-body correlations that would otherwise require very large static multi-determinant expansions.

For each walker $|\phi\rangle$, the trial enters through the AFQMC overlap ratio

$$O_\theta(\phi) = \int \mathrm{d}\mathbf{x} \langle\tilde{\psi}_I|\tilde{U}^\dagger(\mathbf{x})|\phi\rangle \tag{13}$$

and the corresponding mixed local energy

$$E^\theta_{\mathrm{loc}}(\phi) = \frac{\displaystyle\int \mathrm{d}\mathbf{x} \left\langle\tilde{\psi}_I\right|\tilde{U}^\dagger(\mathbf{x})\hat{H}|\phi\rangle}{\displaystyle\int \mathrm{d}\mathbf{x} \left\langle\tilde{\psi}_I\right|\tilde{U}^\dagger(\mathbf{x})|\phi\rangle}. \tag{14}$$

Each term $\tilde{U}(\mathbf{x})\left|\tilde{\psi}_I\right\rangle$ is itself a Slater determinant, so the stochastic sampling over $\mathbf{x}$ produces a sequence of determinants that collectively act as a dynamically updated multi-determinant trial wave function.

During AFQMC propagation, the phaseless constraint is applied using the phase of the sampled overlap ratio,

$$w \to w\, \max(0, \cos\Delta\theta), \tag{15}$$

$$\Delta\theta = \arg O_\theta(\phi_{n+1}) - \arg O_\theta(\phi_n). \tag{16}$$

Here ϕ_n denotes the Slater-determinant walker after n steps of imaginary-time projection, with ϕ_{n+1} obtained from ϕ_n by applying a single AFQMC propagator. In addition to this "right-hand" constraint associated with the update $\phi_n \to \phi_{n+1}$, the stochastic sampling of the trial $\langle\psi_\theta|$ introduces a second overlap ratio when the Metropolis chains attached to each walker are re-equilibrated; following the original stochastic-trial implementation, we apply the same cosine projection to this "left-hand" ratio to suppress phase noise from the trial update, and in practice the two phase angles can be combined into a single effective $\Delta\theta$ in the small-angle limit.:contentReference[oaicite:0]index=0 Meanwhile, $\mathrm{Re}[E^\theta_{\mathrm{loc}}]$ contributes to the mixed estimator for the total energy.

Because the effective trial seen by AFQMC consists of a large number of on-the-fly determinants generated through the auxiliary-field sampling, the resulting constraint is substantially more flexible than a conventional single-determinant or static multi-determinant trial. This dynamical representation significantly improves the stability of the phaseless projection and enhances accuracy across challenging correlated systems.

V. ACKNOWLEDGMENTS

VI. COMPETING INTERESTS

The authors declare no competing interests.

[1] Z.-Y. Xiao, T. Xiang, Z. Lu, Y. Chen, and S. Zhang, Implementing advanced trial wave functions in fermion quantum monte carlo via stochastic sampling, The Journal of Chemical Physics **163**, 164109 (2025).

[2] Z.-Y. Xiao, B. Kan, H. Ma, B. Zhao, and H. Shang, Nnqs-afqmc: Neural network quantum states enhanced fermionic quantum monte carlo, Journal of Chemical Theory and Computation **21**, 9587 (2025).

[3] Z.-Y. Xiao, H. Shi, and S. Zhang, Interfacing branching random walks with metropolis sampling: Constraint release in auxiliary-field quantum monte carlo, Journal of Chemical Theory and Computation **19**, 6782 (2023).

[4] Y. Chen, L. Zhang, W. E, and R. Car, Hybrid auxiliary field quantum monte carlo for molecular systems, Journal of Chemical Theory and Computation **19**, 4484 (2023).

[5] J. A. Pople, Nobel lecture: Quantum chemical models, Rev. Mod. Phys. **71**, 1267 (1999).

[6] W. Kohn, Nobel lecture: Electronic structure of matter—wave functions and density functionals, Rev. Mod. Phys. **71**, 1253 (1999).

[7] P. Hohenberg and W. Kohn, Inhomogeneous electron gas, Phys. Rev. **136**, B864 (1964).

[8] W. Kohn and L. J. Sham, Self-consistent equations including exchange and correlation effects, Phys. Rev. **140**, A1133 (1965).

[9] R. J. Bartlett and M. Musiał, Coupled-cluster theory in quantum chemistry, Rev. Mod. Phys. **79**, 291 (2007).

[10] T. D. Crawford and H. F. Schaefer III, An introduction to coupled cluster theory for computational chemists, in Reviews in Computational Chemistry (John Wiley Sons, Ltd, 2000) pp. 33–136.

[11] C. David Sherrill and H. F. Schaefer, The configuration interaction method: Advances in highly correlated approaches (Academic Press, 1999) pp. 143–269.

[12] A. A. Holmes, N. M. Tubman, and C. J. Umrigar, Heat-bath configuration interaction: An efficient selected configuration interaction algorithm inspired by heat-bath sampling., Journal of chemical theory and computation **12 8**, 3674 (2016).

[13] S. Sharma, A. A. Holmes, G. Jeanmairet, A. Alavi, and C. J. Umrigar, Semistochastic heat-bath configuration interaction method: Selected configuration interaction with semistochastic perturbation theory, Journal of Chemical Theory and Computation **13**, 1595 (2017).

[14] S. R. White, Density matrix formulation for quantum renormalization groups, Phys. Rev. Lett. **69**, 2863 (1992).

[15] G. K.-L. Chan, A. Keselman, N. Nakatani, Z. Li, and S. R. White, Matrix product operators, matrix product states, and ab initio density matrix renormalization group algorithms, Journal of Chemical Physics **145**, 10.1063/1.4955108 (2016).

[16] G. K.-L. Chan and S. Sharma, The density matrix renormalization group in quantum chemistry, Annual Review of Physical Chemistry **62**, 465 (2011).

[17] A. Georges, G. Kotliar, W. Krauth, and M. J. Rozenberg, Dynamical mean-field theory of strongly correlated fermion systems and the limit of infinite dimensions, Rev. Mod. Phys. **68**, 13 (1996).

[18] G. Kotliar, S. Y. Savrasov, K. Haule, V. S. Oudovenko, O. Parcollet, and C. A. Marianetti, Electronic structure calculations with dynamical mean-field theory, Rev. Mod. Phys. **78**, 865 (2006).

[19] D. Zgid and G. K.-L. Chan, Dynamical mean-field theory from a quantum chemical perspective, The Journal of Chemical Physics **134**, 094115 (2011).

[20] G. Knizia and G. K.-L. Chan, Density matrix embedding: A simple alternative to dynamical mean-field theory, Phys. Rev. Lett. **109**, 186404 (2012).

[21] G. Knizia and G. K.-L. Chan, Density matrix embedding: A strong-coupling quantum embedding theory, Journal of Chemical Theory and Computation **9**, 1428 (2013).

[22] G. Carleo and M. Troyer, Solving the quantum many-body problem with artificial neural networks, Science **355**, 602 (2017).

[23] D. Luo and B. K. Clark, Backflow transformations via neural networks for quantum many-body wave functions, Phys. Rev. Lett. **122**, 226401 (2019).

[24] D. Pfau, J. S. Spencer, A. G. D. G. Matthews, and W. M. C. Foulkes, Ab initio solution of the many-electron schrödinger equation with deep neural networks, Phys. Rev. Res. **2**, 033429 (2020).

[25] J. Hermann, Z. Schätzle, and F. Noé, Deep-neural-network solution of the electronic schrödinger equation, Nature Chemistry **12**, 891 (2020).

[26] R. Li, H. Ye, D. Jiang, X. Wen, C. Wang, Z. Li, X. Li, D. He, J. Chen, W. Ren, and L. Wang, A computational framework for neural network-based variational monte carlo with forward laplacian, Nature Machine Intelligence **6**, 209 (2024).

[27] I. von Glehn, J. S. Spencer, and D. Pfau, A self-attention ansatz for ab-initio quantum chemistry (2023), arXiv:2211.13672 [physics.chem-ph].

[28] F. Becca and S. Sorella, Quantum Monte Carlo Approaches for Correlated Systems (Cambridge University Press, 2017).

[29] W. M. C. Foulkes, L. Mitas, R. J. Needs, and G. Rajagopal, Quantum monte carlo simulations of solids, Rev. Mod. Phys. **73**, 33 (2001).

[30] S. Zhang, J. Carlson, and J. E. Gubernatis, Constrained path quantum monte carlo method for fermion ground states, Phys. Rev. Lett. **74**, 3652 (1995).

[31] S. Zhang, J. Carlson, and J. E. Gubernatis, Constrained path monte carlo method for fermion ground states, Phys. Rev. B **55**, 7464 (1997).

[32] S. Zhang and H. Krakauer, Quantum monte carlo method using phase-free random walks with slater determinants, Phys. Rev. Lett. **90**, 136401 (2003).

[33] M. Motta and S. Zhang, Ab initio computations of molecular systems by the auxiliary-field quantum monte carlo method, WIREs Computational Molecular Science **8**, e1364 (2018).

[34] H. Shi and S. Zhang, Some recent developments in auxiliary-field quantum monte carlo for real materials, The Journal of Chemical Physics **154**, 024107 (2021).

[35] H. Shi and S. Zhang, Some recent developments in auxiliary-field quantum monte carlo for real materials, The Journal of Chemical Physics **154**, 10.1063/5.0031024 (2021).

[36] W. A. Al-Saidi, S. Zhang, and H. Krakauer, Bond breaking with auxiliary-field quantum monte carlo, The Journal of Chemical Physics **127**, 144101 (2007).

[37] A. Mahajan, J. Lee, and S. Sharma, Selected configuration interaction wave functions in phaseless auxiliary field quantum monte carlo, The Journal of Chemical Physics **156**, 174111 (2022).

[38] T. Jiang, B. O'Gorman, A. Mahajan, and J. Lee, Unbiasing fermionic auxiliary-field quantum monte carlo with matrix product state trial wavefunctions, Phys. Rev. Res. **7**, 013038 (2025).

[39] D. Danilov, B. Ganoe, M. Munyi, and J. Shee, Capturing strong correlation in molecules with phaseless auxiliary-field quantum monte carlo using generalized hartree–fock trial wave functions, Journal of Chemical Theory and Computation **21**, 1136 (2025).

[40] Z.-Y. Xiao, H. Shi, and S. Zhang, Pseudo-bcs wave function from density matrix decomposition: Application in auxiliary-field quantum monte carlo, Phys. Rev. Res. **3**, 013065 (2021).

[41] J. S. Kurian, H.-Z. Ye, A. Mahajan, T. C. Berkelbach, and S. Sharma, Toward linear scaling auxiliary-field quantum monte carlo with local natural orbitals, Journal of Chemical Theory and Computation **20**, 134 (2024).

[42] H. Shi and S. Zhang, Symmetry in auxiliary-field quantum monte carlo calculations, Phys. Rev. B **88**, 125132 (2013).

[43] H. Shi, C. A. Jiménez-Hoyos, R. Rodríguez-Guzmán, G. E. Scuseria, and S. Zhang, Symmetry-projected wave functions in quantum monte carlo calculations, Phys. Rev. B **89**, 125129 (2014).

[44] W. J. Huggins, B. A. O'Gorman, N. C. Rubin, D. R. Reichman, R. Babbush, and J. Lee, Unbiasing fermionic quantum monte carlo with a quantum computer, Nature **603**, 416 (2022).

[45] W. Purwanto, S. Zhang, and H. Krakauer, An auxiliary-field quantum monte carlo study of the chromium dimer, The Journal of Chemical Physics **142**, 064302 (2015).

[46] Y.-Y. He, M. Qin, H. Shi, Z.-Y. Lu, and S. Zhang, Finite-temperature auxiliary-field quantum monte carlo: Self-consistent constraint and systematic approach to low temperatures, Phys. Rev. B **99**, 045108 (2019).

[47] A. Mahajan, J. H. Thorpe, J. S. Kurian, D. R. Reichman, D. A. Matthews, and S. Sharma, Beyond ccsd(t) accuracy at lower scaling with auxiliary field quantum monte carlo, Journal of Chemical Theory and Computation **21**, 1626 (2025).

[48] C. J. Umrigar, Observations on variational and projector monte carlo methods, The Journal of Chemical Physics **143**, 164105 (2015).

[49] W. Ren, W. Fu, X. Wu, and J. Chen, Towards the ground state of molecules via diffusion monte carlo on neural networks, Nature Communications **14**, 1860 (2023).

[50] A. Karton, S. Daon, and J. M. Martin, W4-11: A high-confidence benchmark dataset for computational thermochemistry derived from first-principles w4 data, Chemical Physics Letters **510**, 165 (2011).

[51] S. Sorella, Systematically improvable mean-field variational ansatz for strongly correlated systems: Application to the hubbard model, Phys. Rev. B **107**, 115133 (2023).

[52] R. Levy, M. A. Morales, and S. Zhang, Automatic order detection and restoration through systematically improvable variational wave functions, Phys. Rev. Res. **6**, 013237 (2024).

[53] J. Bradbury, R. Frostig, P. Hawkins, M. J. Johnson, C. Leary, D. Maclaurin, G. Necula, A. Paszke, J. VanderPlas, S. Wanderman-Milne, and Q. Zhang, JAX: composable transformations of Python+NumPy programs (2018).

[54] J. Lee, H. Q. Pham, and D. R. Reichman, Twenty years of auxiliary-field quantum monte carlo in quantum chemistry: An overview and assessment on main group chemistry and bond-breaking, Journal of Chemical Theory and Computation **18**, 7024 (2022).

[55] Y. J. Bomble, J. F. Stanton, M. Kállay, and J. Gauss, Coupled-cluster methods including noniterative corrections for quadruple excitations, The Journal of Chemical Physics **123**, 054101 (2005).

[56] Z. Sukurma, M. Schlilpf, M. Humer, A. Taheridehkhordi, and G. Kresse, Benchmark phaseless auxiliary-field quantum monte carlo method for small molecules, Journal of Chemical Theory and Computation **19**, 4921 (2023).

[57] A. Tajti, P. G. Szalay, A. G. Császár, M. Kállay, J. Gauss, E. F. Valeev, B. A. Flowers, J. Vázquez, and J. F. Stanton, Heat: High accuracy extrapolated ab initio thermochemistry, The Journal of Chemical Physics **121**, 11599 (2004).

[58] A. Karton, N. Sylvetsky, and J. M. L. Martin, W4-17: A diverse and high-confidence dataset of atomization energies for benchmarking high-level electronic structure methods, Journal of Computational Chemistry **38**, 2063 (2017).

[59] Q. Lu and K. A. Peterson, Correlation consistent basis sets for lanthanides: The atoms la–lu, J. Chem. Phys. **145**, 054111 (2016).

[60] R. Feng and K. A. Peterson, Correlation consistent basis sets for actinides. ii. the atoms ac and np–lr, J. Chem. Phys. **147**, 084108 (2017).

[61] S. C. North and A. K. Wilson, Ab initio composite approaches for heavy element energetics: Ionization potentials for the actinide series of elements, J. Phys. Chem. A **126**, 3027 (2022).

[62] K. T. Williams, Y. Yao, J. Li, L. Chen, H. Shi, M. Motta, C. Niu, U. Ray, S. Guo, R. J. Anderson, J. Li, L. N. Tran, C.-N. Yeh, B. Mussard, S. Sharma, F. Bruneval, M. van Schilfgaarde, G. H. Booth, G. K.-L. Chan, S. Zhang, E. Gull, D. Zgid, A. Millis, C. J. Umrigar, and L. K. Wagner (Simons Collaboration on the Many-Electron Problem), Direct comparison of many-body methods for realistic electronic hamiltonians, Phys. Rev. X **10**, 011041 (2020).

[63] J. Shee, B. Rudshteyn, E. J. Arthur, S. Zhang, D. R. Reichman, and R. A. Friesner, On achieving high accuracy in quantum chemical calculations of 3 d transition metal-containing systems: A comparison of auxiliary-field quantum monte carlo with coupled cluster, density functional theory, and experiment for diatomic molecules, J. Chem. Theory Comput. **15**, 2346 (2019).

[64] Z. Li, Z. Lu, R. Li, X. Wen, X. Li, L. Wang, J. Chen, and W. Ren, Spin-symmetry-enforced solution of the many-body schrödinger equation with a deep neural network, Nature Computational Science **4**, 910 (2024).

[65] P. B. Szabó, Z. Schätzle, M. T. Entwistle, and F. Noé, An improved penalty-based excited-state variational monte carlo approach with deep-learning ansatzes, Journal of Chemical Theory and Computation **20**, 7922 (2024).